# Microstructure of (Ga,Mn)As/GaAs digital ferromagnetic heterostructures

X. Kong,[a] A. Trampert, X. X. Guo, D. Kolovos-Vellianitis, L. Däweritz, and K. H. Ploog
*Paul-Drude-Institut für Festkörperelektronik, Hausvogteiplatz 5-7, D-10117 Berlin, Germany*

(Received 1 December 2004; accepted 16 February 2005; published online 22 April 2005)

We report on the microstructure of (Ga,Mn)As digital ferromagnetic heterostructures grown on GaAs (001) substrates by low-temperature molecular-beam epitaxy. The Mn concentration and the $As_4$/Ga beam equivalent pressure (BEP) ratio are varied in the samples containing periods of Mn sheets separated by thin GaAs spacer layers. Transmission electron microscopy studies reveal that decreasing the Mn doping concentration and reducing the BEP ratio lead to smaller composition fluctuations of Mn and more homogeneous (Ga,Mn)As layers with abrupt interfaces. Planar defects are found as the dominant defect in these heterostructures and their density is related to the magnitude of the composition fluctuation. These defects show a noticeable anisotropy in the morphologic distribution parallel to the orthogonal [110] and $[1\bar{1}0]$ direction. Along the $[1\bar{1}0]$ direction, they are stacking faults, which are preferentially formed in V-shaped pairs and nucleate at the interfaces between (Ga,Mn)As and GaAs layers. Along the [110] direction, the planar defects are isolated thin twin lamellae. The character of the planar defects and their configuration are analyzed in detail. © *2005 American Institute of Physics*. [DOI: 10.1063/1.1889225]

## I. INTRODUCTION

The recent discovery of hole-mediated ferromagnetism in (Ga,Mn)As[1] has attracted much attention, in particular due to the possibility of adding magnetic functionality to GaAs-based semiconductor heterosystems which, in the last few years, have been the benchmark for innovative physics and high-speed optoelectronic devices. Taking into account the advantage of the delta-doping technique, so-called (Ga,Mn)As digital ferromagnetic heterostructures (DFHs) can be tailored with monolayers of Mn atoms separated by GaAs spacer layers.[2,3] The DFHs are believed to induce a high Curie temperature ($T_c$) due to the locally confined high Mn doping concentration. However, because of the limited incorporation of Mn in GaAs and the thermodynamic driving force to phase separation (hexagonal MnAs phase), the DFHs have to be grown in a metastable growth regime using low-temperature molecular-beam epitaxy (LT-MBE). As a result, the quality of the heterostructures is very sensitive to the Mn doping concentration and the LT-MBE growth conditions. In fact, on the one hand, LT growth leads to the formation of intrinsic point defects, such as As antisites and Mn interstitials, affecting the ferromagnetic behavior.[4,5] On the other hand, the level of the Mn doping concentration and the specific growth conditions can influence the Mn diffusion and thus determine the structural perfection of the interfaces. According to recent theoretical work, uniform and sharp interfaces are, however, essential for achieving high $T_c$ values.[6] Furthermore, an inhomogeneity of the lateral Mn distribution can result in the formation of extended defects, which may also affect the ferromagnetism, although the exact influence of the microstructure is still unknown. Therefore, the influence of the Mn doping concentration and the LT-MBE growth conditions on the resultant microstructure has to be clarified in detail in order to improve the quality of DFHs and, further, to understand their specific magnetic properties.

In the first part of this article, a detailed microstructural investigation is presented based on a series of DFHs grown with different Mn doping concentration and $As_4$/Ga beam equivalent pressure (BEP) ratios. Transmission electron microscopy (TEM) analysis reveals that decreasing the Mn doping concentration and reducing the BEP ratio lead to smaller fluctuations of the Mn distribution at the interfaces, to more homogeneous (Ga,Mn)As layers with abrupt interfaces, and, furthermore, to a lower density of extended defects. The second part deals with a detailed defect characterization, which is a basic requirement for an improved understanding of their influence on the ferromagnetic properties.

## II. EXPERIMENTAL DETAILS

The (Ga,Mn)As DFHs were grown on GaAs (001) substrates by standard solid-source MBE.[7] Briefly, a 450 nm GaAs buffer layer was deposited at 580–600 °C, followed by a cooling step to about 250 °C. Then, a 5 nm GaAs layer was grown at this low temperature, before the DFHs were fabricated by alternately opening the Ga and Mn shutter at constant $As_4$ flux. Finally, the samples were capped with 5 nm GaAs. In-situ reflection high-energy electron diffraction (RHEED) was used to monitor the surface reconstruction during growth. During the Ga and Mn deposition, the streaky RHEED patterns exhibited a $(1\times1)$ [or a $d(4\times4)$] and a weak $(1\times2)$ surface reconstruction, respectively.[7] For the structural analysis, the DFHs were studied by conventional TEM and high-resolution (HR) TEM in plan-view and $\langle110\rangle$ cross-sectional view using a JEOL 3010 microscope operating at 300 kV. The TEM samples were prepared by the standard method, i.e., mechanical grinding, dimpling, and

[a]Author to whom correspondence should be addressed; electronic mail: xkong@pdi-berlin.de

 

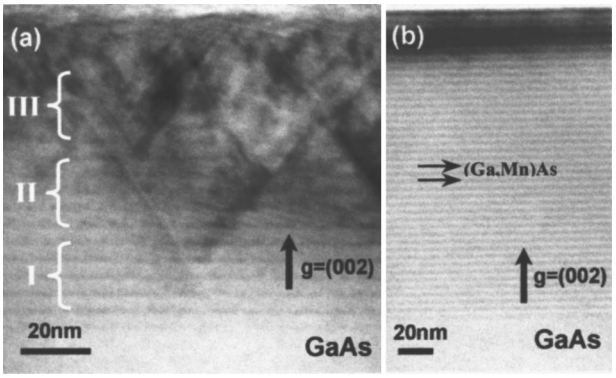


FIG. 1. (a) Cross-sectional (002) bright-field TEM image of the sample containing three superlattices: $[(Mn_{0.75ML}/GaAs_{17ML})_5$, $(Mn_{0.95ML}/GaAs_{17ML})_5$, and $(Mn_{1.15ML}/GaAs_{17ML})_5]$. The density of planar defects increases with increasing Mn doping concentration. (b) The (002) bright-field cross-sectional TEM image of $(Mn_{0.4ML}/GaAs_{17ML})_5$ demonstrates that there are no planar defects found for 0.4 ML Mn sheets.

ion-beam thinning at room temperature in a Gatan precision ion polishing system using 3 keV $Ar^+$-ions and sputtering incident angle of 3°–5°.

In order to study the influences of the Mn doping concentration and the BEP ratio on the resultant microstructure, various DFHs were grown by LT-MBE. The samples are divided into two groups: (i) with different Mn doping concentrations, and (ii) with varying BEP ratio. All MBE samples contain the same superlattice sequence of $(Mn_{x\mathrm{ML}}/GaAs_{y\mathrm{ML}})_z$, i.e., they are composed of $z$ periods of a nominal $x$ ML Mn sheet between $y$ ML GaAs spacer layers.

## III. RESULTS AND DISCUSSION

### A. Effect of Mn concentration variation

Figure 1(a) shows a cross-sectional bright-field TEM image of the sample containing three subsequently grown superlattices with nominally increasing Mn doping concentrations: I $(Mn_{0.75ML}/GaAs_{17ML})_5$, II $(Mn_{0.95ML}/GaAs_{17ML})_5$, and III $(Mn_{1.15ML}/GaAs_{17ML})_5$. Under the $\vec{g}=(002)$ imaging condition, which is sensitive to the chemical composition of the zinc-blende compound, a well-defined superlattice structure is observed for superlattice I and II. The dark lines in the micrographs parallel to the (002) planes correspond to several monolayers with high Mn content. This result is in agreement with our HRTEM lattice images,[8] which reveal coherent zinc-blende (Ga,Mn)As layers between the GaAs spacers. In our TEM samples, no indications are found for hexagonal MnAs precipitates. However, planar defects exist on the corresponding {111} planes. Their density increases drastically from superlattice I to superlattice III, i.e., with increasing Mn concentration. Moreover, in superlattice III with the highest nominal Mn doping concentration, the planar defect density is so large that the (Ga,Mn)As layer sequence becomes invisible. Additionally, it is remarkable that most of the planar defects nucleate at the interface between the (Ga,Mn)As and GaAs layers, implying that epitaxial strain due to Mn incorporation in the GaAs lattice is responsible for the planar defect generation at this high doping content. Indeed, if reducing the epitaxial strain by lowering the Mn concentration to 0.4 ML, the resulting superlattice structure becomes free of extended defects, as demonstrated in the cross-sectional TEM micrograph of the corresponding $(Mn_{0.4ML}/GaAs_{17ML})_{40}$ sample in Fig. 1(b). This result is in agreement with our plan-view studies.

These results indicate a dilemma: on the one hand, the high Mn doping concentration in the DFHs is preferable because it is significant to provide a high enough hole concentration for achieving strong ferromagnetic coupling; on the other hand, the high Mn doping concentration results in large epitaxial strain and, consequently, in low structural quality of DFHs with a high concentration of extended defects. As a compromise, it is therefore required that the Mn doping concentration has to be controlled so that the density of extended defects is as low as possible. In fact, the formation of extended defects is induced not only by the large lattice mismatch between bulk (Ga,Mn)As and GaAs, but also by the high local built-in strain due to the imperfections at the interfaces. These imperfections at the interfaces correspond to the fluctuations in Mn distribution originating from effects of the applied growth condition on the growing surface and, thus, the interface structure.[8] Therefore, the influence of the growth conditions on the interface structure has to be analyzed in more detail.

### B. Effect of BEP ratio

In order to investigate the effect of the growth conditions on the interface structure and the formation of planar defects, two samples were grown at the same Mn doping concentration (0.75 ML) but with $As_4/Ga$ BEP ratios of 5 and 30, respectively. Figures 2(a) and 2(b) display representative $\langle 110\rangle$ cross-sectional TEM images of both samples taken under a $\vec{g}=(002)$ imaging condition. The width of the dark lines in these micrographs reveals that in both cases the fabricated DFHs contain several monolayers of (Ga,Mn)As, pointing to Mn interdiffusion even at this relatively low growth temperature. Moreover, in the sample grown with BEP ratio 5, the interfaces between the (Ga,Mn)As layers and the GaAs spacer layers appear more abrupt and the average thickness of the (Ga,Mn)As layers is smaller compared to the sample grown with BEP ratio 30. On the other hand, in the sample grown with BEP ratio 30, small areas with darker contrast appear in the micrograph along the (Ga,Mn)As layers, indicating the formation of Mn-rich clusters, which are coherent with the GaAs crystal lattice. In contrast, the (Ga,Mn)As layers in a sample grown with BEP ratio 5 are more uniform and homogeneous.

Additionally, Figs. 2(c)–2(f) show that planar defects appear either single and isolated or as combined, V-shaped pairs, depending on the $\langle 110\rangle$ direction. The isolated defects on $(\bar{1}11)$ or $(1\bar{1}1)$ planes are observed end-on along the [110] direction [Figs. 2(c) and 2(d)], whereas the pairs on (111) and $(\bar{1}\bar{1}1)$ planes are viewed end-on along the $[1\bar{1}0]$ direction [Figs. 2(e) and 2(f)]. Two results are remarkable here: First, there is a pronounced anisotropy in the distribution of planar defects along the two orthogonal in-plane $\langle 110\rangle$ directions, where the V-shaped fault pairs and the single faults are only detected in the $[1\bar{1}0]$ and [110] projection, respectively.

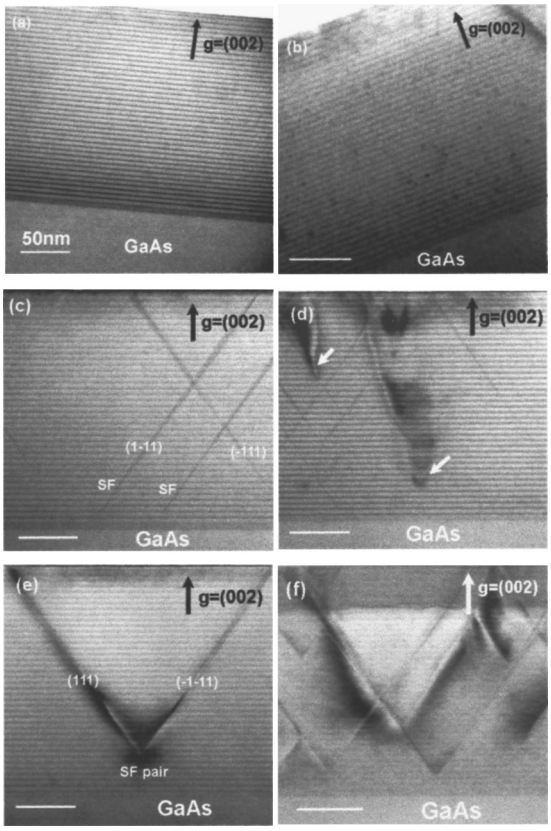


FIG. 2. Cross-sectional (002) bright-field TEM images of $(Mn_{0.75ML}/GaAs_{17ML})_{40}$ with $As_4/Ga$ BEP ratio of 5 (left) and 30 (right), taken near defect-free regions (a) and (b), and defect-containing regions (c)–(f). The images (c) and (d), are taken near the $[110]$ axis and (e) and (f) near $[1\bar{1}0]$ axis, respectively. The $[110]$ and $[1\bar{1}0]$ directions were determined by means of convergent-beam electron diffraction, Ref. 9. The dark and triangle-like contrasts in (d), marked by arrows, are related to SF pairs on the (111) and $(\bar{1}\bar{1}\bar{1})$ planes, which are projected into the image plane normal to electron beam direction.

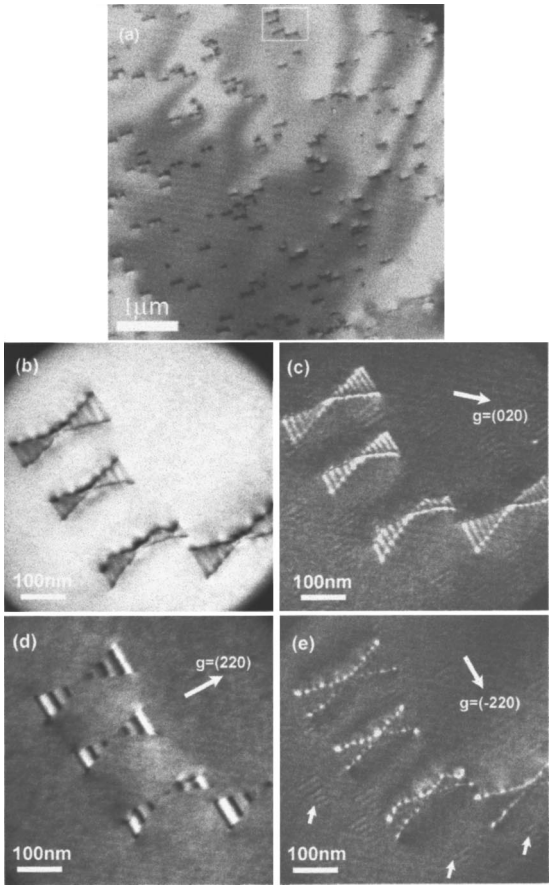


FIG. 3. Plan-view TEM images of SF pairs in $(Mn_{0.75ML}/GaAs_{17ML})_{40}$ with a BEP ratio of 5 taken near the $[001]$ zone axis: (a) and (b) bright-field, (c), (d), and (e) dark-field images under $\vec{g}=(020)$, (220), and $(\bar{2}20)$ weak-beam conditions, respectively. The isolated planar defects with weak diffraction contrast are marked by arrows in (e).

Second, the defect density is drastically reduced in the sample grown with the lower BEP ratio. This result is in agreement with our plan-view observation.

In conclusion, the BEP flux ratio critically affects the lateral Mn distribution at the interfaces. The local atomic configuration results in composition fluctuations along the (Ga,Mn)As layers connected with a pronounced interface roughness. The higher $As_4/Ga$ BEP ratio leads to a larger interface undulation and to a larger density of Mn-rich clusters. Due to the higher local strain at these locations, they act as preferential sites for the nucleation of planar defect pairs.

### C. Defect characterization

The exact knowledge of the character of a structural defect is a basic requirement to be able to further understand its effect on the ferromagnetic properties of these DFHs. Therefore, we have analyzed the specific nature of the extended defects in more detail. The plan-view bright-field image recorded at low magnification in Fig. 3(a) shows an overview of the $(Mn_{0.75ML}/GaAs_{17ML})_{40}$ DFHs grown with a BEP ratio of 5, revealing a characteristic fringe contrast [cf. Fig. 3(b)] with a density of $4\times10^8$ $cm^{-2}$, which is 3–4 times less compared to the sample grown with a BEP ratio 30. The high-magnification images in Figs. 3(c)–3(e) of the marked region were taken with imaging vectors $\vec{g}=(020)$, (220), and $(\bar{2}20)$ near the $[001]$ zone axis, respectively. The fringe contrast observed in these images is typical for planar stacking faults (SFs), in agreement with the cross-sectional TEM results. Additionally, three results are notable: (i) the intersecting line length between the two coupled SFs was measured to be 2–3 nm; (ii) the SF pairs were proved to be of extrinsic type according to the specific fringe contrast measured in Fig. 3(d);[10] (iii) the diffraction contrast of isolated planar defects is found to be very weak, marked by arrows in Fig. 3(e). Indeed, this weak contrast originates from thin twin lamellae, as shown by the following investigation.

#### *1. Stacking fault pair*

In the zinc-blende structure, there are two possible displacement vectors for SFs given by $\vec{R}=\frac{1}{3}\langle111\rangle$ and $\vec{R}=\frac{1}{6}\langle211\rangle$. They are bounded by Frank partial dislocations (PDs) with Burgers vector $\vec{b}=\frac{1}{3}\langle111\rangle$, and Shockley PDs with Burgers vector $\vec{b}=\frac{1}{6}\langle211\rangle$, respectively. In order to determine the character of the PDs bounding the (111) and $(\bar{1}\bar{1}\bar{1})$ SF pairs, the samples had to be tilted close to the $[114]$ and $[\bar{1}\bar{1}4]$ zone axes, where the most conclusive results about

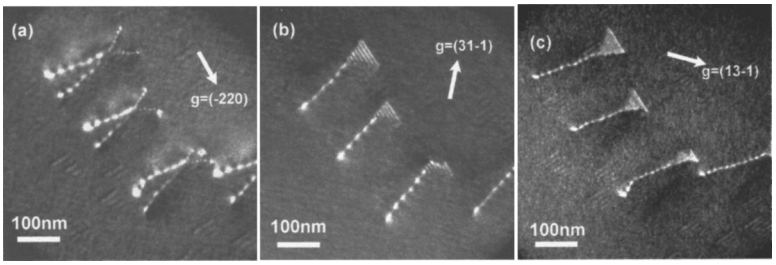


FIG. 4. Plan-view dark-field TEM images of $(Mn_{0.75ML}/GaAs_{17ML})_{40}$ with a BEP ratio of 5, taken near the [114] zone axis with: (a) $\vec{g}=(\bar{2}20)$, (b) $\vec{g}=(31\bar{1})$, and (c) $\vec{g}=(13\bar{1})$.

the Burgers vectors can be obtained from the plan-view images taken with different imaging conditions.

Figures 4(a)–4(c) show dark-field images of SF pairs taken with various diffraction conditions near the [114] zone axis. The PDs visible as four white dotted lines at each SF pairs in Fig. 4(a) clearly demonstrate that they all are of the Shockley type, because those of the Frank type would be invisible under the $\vec{g}=(\bar{2}20)$ imaging condition (cf. Table I). Figures 4(b) and 4(c), taken under a $\vec{g}=(31\bar{1})$ and a $\vec{g}=(13\bar{1})$ imaging condition, respectively, reveal no contrast for the PDs of SFs in the $(\bar{1}11)$ plane, indicating that their Burgers vectors are $\vec{b}_1=\frac{1}{6}[2\bar{1}\bar{1}]$ and $\vec{b}_2=\frac{1}{6}[1\bar{2}1]$ according to the $\vec{g}\cdot\vec{b}$ criterion (Table I). Similarly, the Burgers vectors of PDs in the $(\bar{1}11)$ plane can be determined by tilting near the $[\bar{1}14]$ zone axis: $\vec{b}_3=\frac{1}{6}[\bar{2}1\bar{1}]$ and $\vec{b}_4=\frac{1}{6}[\bar{1}21]$. At the intersecting line of the SF pairs, a stair-rod dislocation with $\vec{b}=\frac{1}{6}\langle 110\rangle$ is formed that is sessile on the (001) plane according to the following dislocation reactions: $\vec{b}_1+\vec{b}_4=\frac{1}{6}[\bar{2}1\bar{1}]+\frac{1}{6}[\bar{1}21]=\frac{1}{6}[110]$, and $\vec{b}_2+\vec{b}_3=\frac{1}{6}[1\bar{2}1]+\frac{1}{6}[\bar{2}1\bar{1}]=\frac{1}{6}[\bar{1}10]$, where the negative sign is related to the definition of the line directions.[11] To summarize our experimental results, the arrangement of a SF pair is schematically presented in Fig. 5(a). The appearance of the SF pairs in $[1\bar{1}0]$ cross-sectional and plan-view samples is explained in Figs. 5(b) and 5(c).

In order to understand the mechanism of SF pair generation in DFHs, the cross-sectional view of the original area of the SF pair was also analyzed by HRTEM, as shown in Fig. 6. This HRTEM micrograph reveals the lattice configuration and stacking sequence of the {111} planes near the starting point, indicating that the two coupled SFs meet at the interface between the (Ga,Mn)As and GaAs layers. A detailed comparison of the density of the SF pairs in samples with low and high BEP ratio verifies our statement from the previous paragraph that the inhomogeneity in the lateral Mn distribution, thus the resultant local strain and the specific surface morphology, cause the SF pair formation along the $[1\bar{1}0]$ direction.[8]

### 2. Thin twin lamellae

The weak diffraction contrasts of the isolated planar defects on the $(\bar{1}11)$ or $(1\bar{1}1)$ planes are unexpected for perfect SFs. Therefore, the nature of these extended defects has to be clarified more precisely.

The [110] cross-sectional HRTEM image (Fig. 7) of the isolated planar defect on the $(\bar{1}11)$ plane shows that the boundaries of this kind of planar defect marked by arrows in the inset, exhibit mirror symmetry compared to the rest of the perfect crystal. This is characteristic for twins. The stacking sequence of a twin is •••ABC$\underset{\downarrow}{A}$C$\underset{\downarrow}{B}$ABC•••, where the labels A, B, C denote the various positions of {111} planes in the fcc crystal. Such a thin twin can be considered to be formed by progressive shear operations on subsequent $(\bar{1}11)$ planes produced by Shockley PDs of the same Burgers vector $\vec{R}=\frac{1}{6}[\bar{1}1\bar{2}]$. According to the observation of a large number of twins, the twin thickness is found to comprise no more than four {111} layers. These thin defects and their lattice images are applied to clarify the origin of the weak diffraction contrast in plan-view TEM: when the electrons penetrate through the twin in the plan-view geometry, the total twin displacement vector returns to the perfect crystal structure, and the corresponding total phase shifts $(2\pi\vec{g}\cdot\vec{R})$ turn to zero.[12] Therefore, the diffraction contrast from thin twins with several {111} planes is very weak compared to the case of the SF pairs (Figs. 3 and 4).

TABLE I. $\vec{g}\cdot\vec{b}$ criterion for Burgers vectors of Shockley and Frank partial dislocations on the (111) and $(\bar{1}11)$ planes near the [114] axis.

| | Plane (111) | | | | Plane $(\bar{1}11)$ | | | |
|---|---|---|---|---|---|---|---|---|
| | Shockley | | | Frank | Shockley | | | Frank |
| $\vec{b}$ / $\vec{g}$ | $\frac{1}{6}[2\bar{1}\bar{1}]$ | $\frac{1}{6}[\bar{1}\bar{1}2]$ | $\frac{1}{6}[1\bar{2}1]$ | $\frac{1}{3}[111]$ | $\frac{1}{6}[\bar{2}\bar{1}1]$ | $\frac{1}{6}[112]$ | $\frac{1}{6}[\bar{1}21]$ | $\frac{1}{3}[\bar{1}\bar{1}1]$ |
| $(\bar{2}20)$ | $v^a$ | $i^b$ | $v^a$ | $i^b$ | $v^a$ | $i^b$ | $v^a$ | $i^b$ |
| $(31\bar{1})$ | $v^a$ | $v^a$ | $i^b$ | $v^a$ | $v^a$ | $v^a$ | $v^a$ | $v^a$ |
| $(13\bar{1})$ | $i^b$ | $v^a$ | $v^a$ | $v^a$ | $v^a$ | $v^a$ | $v^a$ | $v^a$ |

[a]Visible.
[b]Invisible.

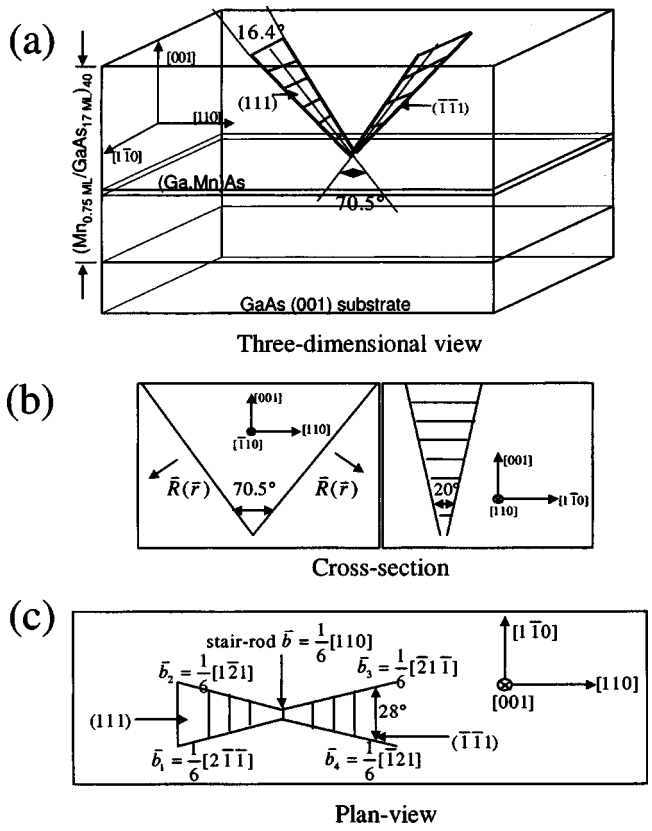


FIG. 5. The three-dimensional arrangement of SF pairs in DFHs (a), and the cross-sectional view (b) and plan view (c) along the $[1\bar{1}0]$ and [001] direction, respectively.

Considering the TEM images in Figs. 2 and 3, the following features of these twins are remarkable: (i) the size of twins increases as they approach the free surface; (ii) the origins are located not only at the interfaces but also within the spacer layers; (iii) the average size is smaller compared to the SF pairs; (iv) the SF pairs start earlier compared to the twins during the MBE growth. According to these results, the twins in these DFHs can be considered as deformation ones,[13] and the mechanism of twin nucleation is supposed to be the following: at the beginning of the LT growth, the high Mn doping concentration and the interface roughness related

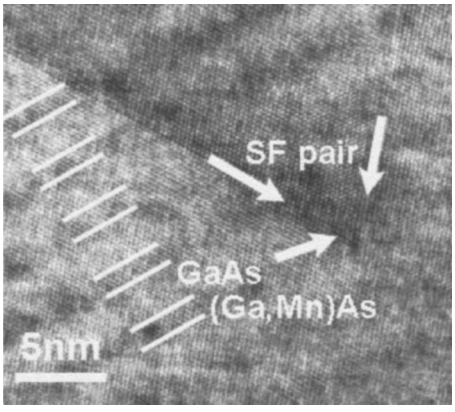


FIG. 6. Cross-sectional HRTEM micrograph of a SF pair in $(Mn_{0.75ML}/GaAs_{17ML})_{40}$, taken along the $[1\bar{1}0]$ zone axis, demonstrating the origin of a SF pair at the interface.

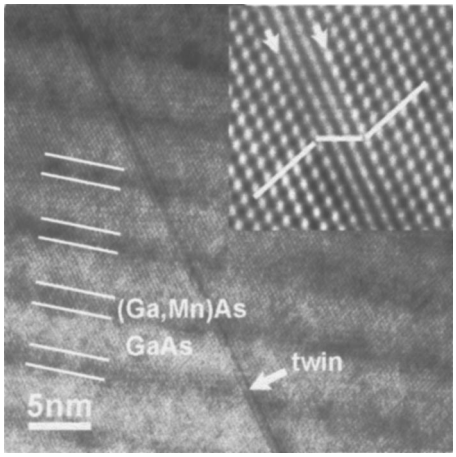


FIG. 7. Cross-sectional [110] HRTEM image of a twin in $(Mn_{0.75ML}/GaAs_{17ML})_{40}$, indicating a thin twin along the $(\bar{1}11)$ plane [(inset) higher magnification].

to the large BEP ratio induce the formation of SF pairs along the $[1\bar{1}0]$ direction as discussed before; these SF pairs and intersecting stair-rod dislocations relieve the local strain along the [110] direction. This fact is responsible for elastic strain in the GaAs spacer layers. Therefore, during the epilayer growth, the accumulating misfit strain along the $[1\bar{1}0]$ direction has to be relaxed, resulting in the shear displacement along the $\frac{1}{6}\langle 211\rangle$ direction of the close-packed planes.

## IV. CONCLUSION

We have investigated a series of DFHs grown with different Mn dopant concentrations and $As_4/Ga$ BEP ratios. The fluctuation of the Mn composition along the (Ga,Mn)As layers and the interface roughness can be minimized by decreasing the nominal Mn doping concentration or by reducing the BEP ratio during LT-MBE growth. Planar defects on the four corresponding {111} planes are observed in samples with higher Mn concentration. These defects show a noticeable anisotropy in density parallel to the orthogonal [110] and $[1\bar{1}0]$ direction, respectively. Along the $[1\bar{1}0]$ direction, the planar defects are SFs preferentially formed as V-shaped pairs. Applying the $\vec{g}\cdot\vec{b}$ criterion, it is demonstrated that the SF pairs are bounded by Shockley PDs with Burgers vectors $\vec{b}=\frac{1}{6}\langle 211\rangle$. The cross-sectional TEM images reveal that the SF pair preferably nucleate at the interface between (Ga,Mn)As and GaAs, due to the high local strain introduced by the Mn composition fluctuation. The isolated planar defects on the $(\bar{1}11)$ and $(1\bar{1}1)$ planes are thin twin lamellae, which contribute to the relaxation of the mismatch strain along the $[1\bar{1}0]$ direction.

[1]H. Ohno, A. Shen, F. Matsukura, A. Oiwa, A. Endo, S. Katsumoto, and Y. Iye, Appl. Phys. Lett. **69**, 363 (1996); H. Ohno, Science **281**, 951 (1998); T. Dietl, H. Ohno, F. Matsukura, J. Cibert, and D. Ferrand, *ibid.* **287**, 1019 (2000), and references therein.
[2]R. K. Kawakami, E. Johnston-Halperin, L. F. Chen, M. Hanson, N. Guébels, J. S. Speck, A. C. Gossard, and D. D. Awschalom, Appl. Phys. Lett. **77**, 2379 (2000).
[3]A. M. Nazmul, S. Sugahara, and M. Tanaka, J. Cryst. Growth **251**, 303 (2003).

[4]K. W. Edmonds *et al.*, Phys. Rev. Lett. **92**, 037201 (2004).
[5]S. Sanvito and N. A. Hill, J. Magn. Magn. Mater. **242–245**, 441 (2002).
[6]J. Fernández-Rossier and L. J. Sham, Phys. Rev. B **64**, 235323 (2001).
[7]X. X. Guo, C. Herrmann, X. Kong, D. Kolovos-Vellianitis, L. Däweritz, and K. H. Ploog, J. Cryst. Growth (in press).
[8]X. Kong, A. Trampert, X. X. Guo, L. Däweritz, and K. H. Ploog, J. Appl. Phys. **97**, 036105 (2005).
[9]J. Tafto and J. C. H. Spence, J. Appl. Crystallogr. **15**, 60 (1982).
[10]D. B. Williams and C. B. Carter, *Transmission Electron Microscopy* (Plenum Press, New York, 1996), p. 386.
[11]J. P. Hirth and J. Lothe, *Theory of Dislocation* (Wiley, New York, 1982).
[12]C. Y. Chen and W. M. Stobbs, Inst. Phys. Conf. Ser. **134**, 417, (1993).
[13]P. D. Brown, Y. Y. Loginov, W. M. Stobbs, and C. J. Humphreys, Philos. Mag. **72**, 39 (1995); X. L. Wei and M. Aindow, Appl. Phys. Lett. **65**, 1903 (1994).